JACS
JOURNAL OF THE AMERICAN CHEMICAL SOCIETY
pubs.acs.org/JACS
Article

Molecular Weight Dependence of Block Copolymer Micelle Fragmentation Kinetics

Julia T. Early, Alison Block, Kevin G. Yager, and Timothy P. Lodge*

Cite This: https://doi.org/10.1021/jacs.1c02147
Read Online

ABSTRACT: The effect of molecular weight (M) on the fragmentation kinetics of micelles formed by 1,2-polybutadiene-*block*-poly(ethylene oxide) (PB-PEO) copolymers was studied in the ionic liquid 1-ethyl-3-methylimidazolium bis(trifluoromethylsulfonyl)imide. A series of six samples, with total M ranging from 10^4 to 10^5 g mol^{-1} and nearly constant composition ($f_{PEO} \approx 0.4$), were examined; all six formed spherical micelles with PEO coronas. Nonequilibrium PB-PEO micelles were prepared by direct dissolution, a process that systematically produces nanoparticles with mean aggregation numbers more than twice the equilibrium values. When subjected to high temperature annealing (170 °C), the average micelle radius was found to decrease substantially, as determined by temperature-jump dynamic light scattering (T-jump DLS) and time-resolved small-angle X-ray scattering (TR-SAXS). The characteristic fragmentation times (τ) were found to increase strongly with increasing degree of polymerization N, as $\tau \sim N^{1.8}$. This result compares favorably with the prediction of a previously untested model.

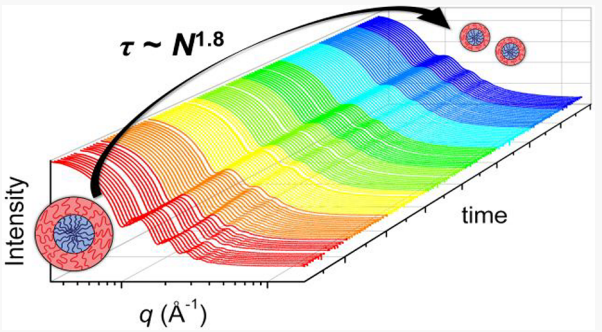

INTRODUCTION

Diblock copolymers self-assemble into a variety of micellar structures in the presence of a block-selective solvent, i.e., a solvent that dissolves one block and not the other. Block copolymer (BCP) micelles are utilized in a wide range of applications including ion gels,[1,2] drug or gene delivery,[3,4] nanolithography,[5] and viscosity modification.[6] Because of the versatility of BCP micelles from an applications perspective, their dynamics and equilibration kinetics in solution are of interest, yet these processes remain less well understood in comparison to their low molecular weight counterparts.[7−10] The thermodynamics of micellization has been studied extensively, both theoretically and experimentally.[11,12] The morphology and size of block copolymer micelles at equilibrium can be tuned by changing the molecular characteristics of the block copolymer itself, such as the core and corona block lengths,[13−16] and the solvent selectivity.[17]

There are five primary processes thought to govern the formation, destruction, and equilibration of block copolymer micelles in solution, namely, (i) *chain exchange*, where individual copolymer chains are exchanged between micelles, (ii) *fragmentation*, where a micelle much larger than the equilibrium aggregation number Q_{eq} breaks up into smaller micelles, (iii) *fusion*, where micelles smaller than Q_{eq} merge together, (iv) micelle *creation*, where individual chains nucleate a new micelle, and (v) *annihilation* of micelles, where a series of chain exchange/fragmentation/fusion events eliminates one micelle. The kinetics of these processes were first modeled by Aniansson, Wall, and co-workers.[18,19] These processes of micellization and equilibration are supported by experimental studies of low molecular weight surfactants[20] and Pluronics.[21−24] Halperin and Alexander developed the first detailed theory of block copolymer micelle dynamics near equilibrium, where chain exchange was considered to be the only plausible equilibration mechanism, as fragmentation and fusion were argued to be much slower.[25,26] Dormidontova proposed a different model that gives scaling predictions for the relaxation times of chain exchange, fragmentation, and fusion.[27] Nyrkova and Semenov focused on the rates of micelle creation and annihilation in response to abrupt changes in conditions such as jumps in temperature.[28]

The molecular weight (M) of diblock copolymers not only affects the equilibrium structure of micelles, but also the dynamics and equilibration kinetics in solution.[8,15,29] The aggregation number Q of a given micelle can vary, and micelle equilibration occurs by some combination of the exchange of individual chains,[7,9,15,30−35] fusion, or fragmentation.[20,22,23,36] Halperin and Alexander proposed that the chain exchange kinetics depends on a characteristic relaxation time, τ, that depends on the core and corona block lengths as $\tau \sim$

Received: February 24, 2021

$N_{core}^{2/25}N_{corona}^{9/5}\exp(E_a/k_BT)$, where E_a is the activation barrier given by $\gamma N_{core}^{2/3}b^2$, where γ is the interfacial tension between the core block and the solvent and b is the monomer size of the core block.[25] Experimentally, the effect of M on micelle chain exchange kinetics has been found to be very strong, with the barrier to exchange increasing linearly with core block degree of polymerization, N_{core}, in contrast to the Halperin-Alexander model.[8,32−34,37,38] Interestingly, it has also been reported that increasing the degree of polymerization of the corona block, N_{corona}, of PS-PEP micelles in squalane could increase the rate of chain exchange by up to 2 orders of magnitude,[15] whereas studies of C_{27}-PEO$_n$ in water showed that increasing N_{corona} had the opposite effect.[8]

Despite the dramatic effect of M on chain exchange, essentially nothing is known experimentally about the influence of M on the kinetics of fragmentation.[36] In general, fragmentation is much slower than chain exchange for micelles that are not too far from equilibrium, thus increasing molecular weight should lead to longer fragmentation time scales.[22,23,36] Techniques including dynamic light scattering (DLS) and time-resolved small-angle X-ray scattering (TR-SAXS) are useful for monitoring changes in micelle size over a wide range of time scales.[39−43] This is primarily due to the relatively short acquisition times required for DLS (i.e., minutes), and particularly for synchrotron SAXS (seconds). Previous work by Kelley et al. showed that micellization of 1,2-polybutadiene-*block*-poly(ethylene oxide) (PB-PEO) in mixtures of tetrahydrofuran and water occurs via a distinct bimodal pathway, and the increase of the average hydrodynamic radius, $\langle R_h\rangle$, was monitored using DLS for as long as 90 days.[41] They concluded that the initial growth of micelles occurs via micelle fusion.[41] Additionally, the combination of DLS and TR-SAXS proves invaluable for determining micelle fragmentation kinetics, as the total micelle radius, i.e., $\langle R_h\rangle$, and the average micelle core radius, $\langle R_{core}\rangle$, are readily determined. In general, chain exchange by itself is not expected to change $\langle R_{core}\rangle$ to a significant extent.[36,44,45]

A theoretical model of the M dependence, specifically the dependence on N_{corona}, of micelle fusion and fragmentation has been reported.[27] Dormidontova proposed a scaling model to account for micellization in systems far from equilibrium, and assumes that micelle fragmentation proceeds by the reverse mechanism as micelle fusion.[27] The relaxation time (τ) for fusion of two micelles with similar aggregation numbers ($Q_1 \leq Q_2$) scales with aggregation number and the degree of polymerization of the corona block as $\tau \sim N_{corona}^{17/5}Q_1^{4/5}Q_2$.[27] The strong N_{corona} dependence on the characteristic time for fusion is attributed to the corona chain deformation during the merging process, where the corona chains of a smaller micelle penetrate into the corona region of a larger micelle. On the basis of this observation for micelle fusion, the fragmentation times for micelles with small aggregation numbers were estimated to scale with $N_{corona}^{17/5}$ as well. The fragmentation time was predicted to scale as $\tau \sim N_{corona}^{9/5}Q^{13/5}$ for micelles with very large aggregation numbers $Q > (cV_{corona})^{5/2}N_{corona}^2$, where c is the micelle concentration and V_{corona} is the molar volume of a corona-forming chain.

Previous work on the micellization of PB-PEO in the ionic liquid (IL) 1-ethyl-3-methylimidazolium bis-(trifluoromethylsulfonyl)imide ([C_2mim][TFSI]) showed that the solution preparation method influences $\langle R_h\rangle$. For micelles prepared by direct dissolution (DD) of the bulk copolymer in the IL, the $\langle R_h\rangle$ of the as-prepared micelles is quite large compared to micelles prepared by the cosolvent method, in which a good solvent is introduced to the solution and slowly evaporated away.[40] For micelles prepared by DD, $\langle R_h\rangle$ decreased to approximately half of the original size when annealed at 170 °C.[40] Further work on this system showed that the time-dependent decrease in $\langle R_h\rangle$ was consistently well-described by a compressed exponential function $\exp(-(t/\tau)^n)$ with an exponent $n \approx 2$, even at lower annealing temperatures (T = 120 °C).[36] To further understand the mechanism, the fragmentation kinetics for one molecular weight of PB-PEO was studied in five 1-alkyl-3-methylimidazolium bis-(trifluoromethylsulfonyl)imide-based ILs ([$C_x$mim][TFSI] where x = 1, 2, 4, 6, and 8).[45] The solvent quality with respect to the PB core-forming block was improved by increasing the length of the alkyl chain on the IL cation, but it was found that the improvement in solvent quality did not affect the fragmentation kinetics of PB-PEO micelles to any significant extent.[45] We previously reported the direct observation of micelle fragmentation for three molecular weights of PB-PEO in [C_2mim][TFSI] using high-temperature liquid-phase transmission electron microscopy, and intermediate structures close to an apparent transition state for micelle fragmentation were observed in situ.[46]

The absence of experimental results on the molecular weight dependence of fragmentation kinetics motivates this work. Here we monitor the fragmentation of PB-PEO in the IL [C_2mim][TFSI] where the total molecular weight of the diblock is varied from 11 to 100 kg mol^{-1} while maintaining a constant volume composition $f_{PEO} \approx 0.4$. The thermal stability and nonvolatility of ILs is exploited here as the solutions can be heated to much higher temperatures than organic solvents, allowing the kinetics of fragmentation to be studied over more accessible time scales.[47]

EXPERIMENTAL SECTION

Synthesis and Characterization. Six PB-PEO copolymers were synthesized by two-step sequential anionic polymerization,[48] as briefly described here. 1,3-Butadiene (Sigma-Aldrich, ≥ 99%) and ethylene oxide (Sigma-Aldrich, ≥ 99.5%) were purified by stirring with vacuum-dried *n*-butyllithium (Sigma-Aldrich, 2.5 M in hexanes) twice for 30 min. Six molecular weights (6−53 kg mol^{-1}) of hydroxyl-terminated 1,2-polybutadiene were synthesized via anionic polymerization of 1,3-butadiene with *sec*-butyllithium in tetrahydrofuran (THF) at −75 °C for 8 h; the polymer chains were end-capped with a single ethylene oxide unit at 27 °C, and the polymerization was terminated by the addition of acidic methanol (1:10 HCl:methanol). A concentrated solution of PB-OH in dichloromethane was precipitated into an excess of cold methanol, isolated via vacuum filtration, and dried under vacuum (<100 mTorr) at 40 °C for 72 h prior to use. PB-PEO diblocks with a nearly constant volume fraction of PEO ($f_{PEO} \approx 0.4$) were prepared by subsequent anionic polymerization of ethylene oxide. The polymerization was performed in THF at 40 °C for 24 h in the presence of PB-OH with potassium naphthalenide. The polymerization was terminated by the addition of acidic methanol (1:10 HCl:methanol). PB-PEO diblocks were freeze-dried in benzene with 0.1 wt % BHT as an antioxidant under vacuum (<100 mTorr) at 27 °C for 24 h prior to use. The samples are denoted BO(x−y), where x and y indicate the number-average molecular weights of the PB and PEO blocks in kg mol^{-1}, respectively. The number-average molecular weight (M_n), dispersity ($Đ$), and f_{PEO} were determined by a combination of size exclusion chromatography (SEC) in THF with a multiangle laser light scattering detector (Wyatt Dawn Heleos II) and ^{1}H nuclear magnetic resonance spectroscopy in $CDCl_3$ (^{1}H NMR, Varian Inova 500) as shown in Table 1. The refractive index detector traces from SEC in THF of all diblocks are shown in the Supporting Information (SI Figure S1). The refractive

https://doi.org/10.1021/jacs.1c02147
J. Am. Chem. Soc. XXXX, XXX, XXX−XXX

Table 1. Characteristics of BO(x−y) Diblock Copolymers[a]

sample	$M_{n,PB}$ (kg mol^{-1})	$M_{n,PEO}$ (kg mol^{-1})	f_{PEO}	$Đ$
BO(6−5)	6.5	5.2	0.38	1.14
BO(8−7)	9.4	7.6	0.38	1.07
BO(10−9)	10	9.4	0.43	1.05
BO(25−22)	25	22	0.41	1.09
BO(27−27)	27	27	0.43	1.06
BO(53−46)	53	46	0.40	1.05

[a]^{1}H NMR spectroscopy in $CDCl_3$ was used to determine the number-average molar mass (M_n) and volume fraction of PEO (f_{PEO}) using bulk densities ρ_{PB} = 0.87 g/cm^3 for PB, and ρ_{PEO} = 1.13 g/cm^3 for PEO. SEC with a multiangle light scattering detector in THF was used to determine the weight-average molar mass (M_w) and molar mass dispersity ($Đ = M_w/M_n$) of the diblocks.

index increment (dn/dc) for a diblock was estimated as the weight-average of the refractive index increments for PB in THF (dn/dc = 0.119 mL/g) and PEO in THF (dn/dc = 0.068 mL/g).[49] The ^{1}H NMR spectra of the diblocks in deuterated chloroform ($CDCl_3$) are shown in Figure S2.

The ionic liquid (IL) 1-ethyl-3-methylimidazolium bis(trifluoromethylsulfonyl)imide ([C_2mim][TFSI]) was synthesized by an anion exchange reaction between 1-ethyl-3-methylimidazolium bromide and lithium bis(trifluoromethylsulfonyl)imide, carried out in water at 70 °C for 24 h.[50] The reaction mixture was diluted with dichloromethane, the aqueous layer was removed, and the organic layer was washed three times with deionized water. The organic layer was stirred on activated charcoal for 24 h. The solution was passed through an alumina column, dichloromethane was removed in vacuo, and [C_2mim][TFSI] was dried under vacuum (<100 mTorr) at 60 °C for 72 h. The dried IL was characterized by ^{1}H, ^{13}C, and ^{19}F NMR spectroscopy in DMSO-d_6. The ^{1}H NMR spectrum for [C_2mim][TFSI] is shown in Figure S3.

Solution Preparation by Direct Dissolution (DD). All solutions were prepared by the direct dissolution (DD) method described here. The desired amounts of PB-PEO and [C_2mim][TFSI] were combined by weight in a 20 mL scintillation vial equipped with a stir bar to obtain a 0.25 wt % solution. The vial was placed in an oil bath and stirred vigorously at 70 °C for 48 h. The resulting DD solutions were slightly blue-tinged for BO(6−5), BO(8−7), and BO(10−9) micelles, whereas those for BO(25−22), BO(27−27), and BO(53−46) were white-tinged.

Dynamic Light Scattering (DLS). Dynamic light scattering measurements were performed on a home-built light scattering setup equipped with a Brookhaven BI-DS photomultiplier mounted to an adjustable goniometer, a Lexel Ar$^+$ laser (λ = 488 nm), and a Brookhaven BI-9000 correlator. During a typical annealing experiment, the temperature was controlled with an index-matching high-temperature silicone oil bath to within ±0.1 °C. To verify the size of the micelles before and after annealing, multiangle light scattering experiments were performed at T = 27 °C with a range of scattering angles θ from 60° to 120°.

Each micelle solution was passed through an 0.45 μm PTFE syringe filter to remove any dust, and subsequently flame-sealed under vacuum (≤70 mTorr) in a dust-free glass tube (I.D. 0.51 cm) to prevent degradation of the block copolymer and to avoid contact with moisture and dust. In an annealing experiment, the oil bath temperature was allowed to equilibrate for 30 min prior to introducing the sample. The normalized intensity autocorrelation function, $g_2(t)$, was measured at θ = 90° as a function of time. For each time point, $g_2(t)$ was acquired for 90 s. The intensity autocorrelation function was converted to the electric field autocorrelation function, $g_1(t)$, via the Siegert relation,[51] which was then fit to a second-order cumulant expansion for single populations to obtain the average decay rate, $\bar{\Gamma}$, and the variance, $\mu_2/\bar{\Gamma}^2$. The mutual diffusion coefficient D_m was calculated from $D_m = \bar{\Gamma}/q^2$, where q is the magnitude of the scattering vector defined by $q = (4\pi n/\lambda_0)\sin(\theta/2)$, where n is the refractive index of [C_2mim][TFSI], and λ_0 is the wavelength of light in a vacuum. For multiangle light scattering experiments, D_m was estimated by taking the slope of the line in plots of $\bar{\Gamma}$ versus q^2 with zero intercept. For dilute solutions, D_m can be used as an approximation of the tracer diffusion coefficient, D_t. This is used to calculate the hydrodynamic radius using the Stokes−Einstein equation:

$$R_h = \frac{k_B T}{6\pi\eta_s D_t} \quad (1)$$

where k_B is the Boltzmann constant, T is the temperature, and $\eta_s(T)$ is the solvent viscosity; η_s(170 °C) = 2.4 kPa·s for [C_2mim][TFSI].[36] The temperature dependence of the viscosity is well described by the Vogel−Fulcher−Tamman equation for [C_2mim][TFSI] and many other ILs.[52−55] Additional analysis of the micelle size distribution was performed by applying the regularized positive exponential sum (REPES) Laplace inversion to the intensity correlation function.[56] Application of this algorithm results in the decay rate distribution, $G(\Gamma)$, which can be expressed in terms of the hydrodynamic radius from eq 1. When the REPES routine showed a sample with a bimodal distribution, $g_1(t)$ was fit to a double-exponential function, shown in eq 2, to obtain the decay rates of each population.

$$g_1(t) = A_1\exp(-\bar{\Gamma}_1 t) + A_2\exp(-\bar{\Gamma}_2 t) \quad (2)$$

Time-Resolved Small Angle X-ray Scattering (TR-SAXS). SAXS experiments were conducted at the 11-BM Complex materials Scattering (CMS) beamline at the National Synchrotron Light Source II (NSLS-II), Brookhaven National Laboratory. Samples of 0.25 wt % PB-PEO directly dissolved in [C_2mim][TFSI] were syringe-filtered into 1.5 mm diameter borosilicate capillaries (Charles Supper Co.) and then placed into a custom 15-capillary temperature-controlled stage. SAXS measurements were conducted with samples under dynamic vacuum at room temperature and 170 °C. Two-dimensional scattering patterns were obtained using a Dectris Pilatus 300k pixel-array detector (pixel size 172 × 172 μm^2) using a 30 s exposure time to 13.5 keV X-rays (λ = 0.918 Å) and a sample-to-detector distance of 2 m. The position where the incident beam hits the capillary was changed throughout a time-resolved experiment to mitigate beam damage effects. The scattering vector q was calibrated using silver behenate. The 2D data were azimuthally averaged to yield 1D scattering patterns as intensity versus q. Due to the presence of higher q upturns in ionic liquid scattering, which has been observed previously, and significant capillary-to-capillary variations, the background (i.e., ionic liquid and capillary scattering) was fit to a power law ($I(q) = A + Bq^{-m}$, where $2 \le m \le 4$) and subtracted from the solution scattering data..[57] The background-corrected intensity traces were fit using an established block copolymer micelle model.[58,59] In this model, the scattering intensity is defined as follows:

$$I(q) = \int D(R_{core})[P_{mic}(q) + A^2_{mic}(q)(S(q) - 1)]dR_{core} \quad (3)$$

where R_{core} is the micelle core radius with distribution $D(R_{core})$, $P_{mic}(q)$ is the spherical form factor for the micelle core,[58] $A_{mic}(q)$ is the form factor amplitude, and $S(q)$ is the hard-sphere structure factor with the Percus−Yevick closure.

SAXS experiments for the bulk BO copolymers were conducted at the 5-ID-D beamline of the Dupont-Northwestern-Dow Collaborative Access Team (DND-CAT) at the Advanced Photon Source, Argonne National Laboratory. All samples were hermetically sealed in aluminum DSC pans under argon with <0.1 wt % BHT as an antioxidant. The samples were annealed at 70 °C for 10 min prior to measurement. SAXS measurements of bulk polymers were conducted at 70 °C. Two-dimensional scattering patterns were obtained using a Rayonix MX170-HS CCD area detector using a 0.5 s exposure time to X-rays with a wavelength of λ = 0.729 Å and a sample-to-detector distance of 8.5 m. The 2D data were azimuthally averaged to yield 1D scattering patterns as intensity versus q.

https://doi.org/10.1021/jacs.1c02147
J. Am. Chem. Soc. XXXX, XXX, XXX−XXX

RESULTS AND DISCUSSION

Initial and Final Micelle Dimensions. SAXS and DLS were used to determine the effect of molecular weight on the size of micelles, both as prepared by direct dissolution and also at steady-state after annealing at 170 °C. The initial size of micelles prepared by DD and after a *T*-jump to 170 °C were determined by multiangle DLS and SAXS, in terms of the overall micelle radius R_h and the micelle core radius R_{core}, respectively. The overall radii were determined by fitting the intensity autocorrelation function from DLS to a second order cumulant expansion. The radii increased monotonically with increasing *M*, as seen in SI Figures S4 and S5. REPES analysis of DLS data, shown in Figure S4, for the as-prepared and steady-state $\langle R_h \rangle$ of 0.25 wt % PB-PEO in $[C_2mim][TFSI]$ corroborates the fitting results in that the $\langle R_h \rangle$ decreases after annealing at 170 °C for all molecular weights. The percent decrease in $\langle R_h \rangle$ after long-time annealing at 170 °C was 31%, 36%, 33%, 17%, 25%, and 29% for BO(6−5), BO(8−7), BO(10−9), BO(25−22), BO(27−27), and BO(53−46), respectively.

To determine the effect of *M* on R_{core}, SAXS was performed at room temperature before and after annealing at 170 °C. The background corrected scattering intensity traces versus *q* for the as-prepared and steady-state micelles are shown in Figure 1a and 1b, respectively. The as-prepared micelles for all polymers, except for BO(53−46), are well-defined spheres. This is confirmed by the distinct first minimum in the form factor and oscillations at higher *q* values, which generally reflect a narrow size distribution and a modest interfacial width at the core−corona interface.[58,60] The increased size dispersity of BO(53−46) micelles may be due to the fixed time used to prepare the solutions, and longer dissolution times may be required to obtain more narrowly distributed initial micelles. Similarly, well-defined smaller spherical micelles are obtained after annealing at 170 °C, as shown in Figure 1b, for all but the largest polymer.

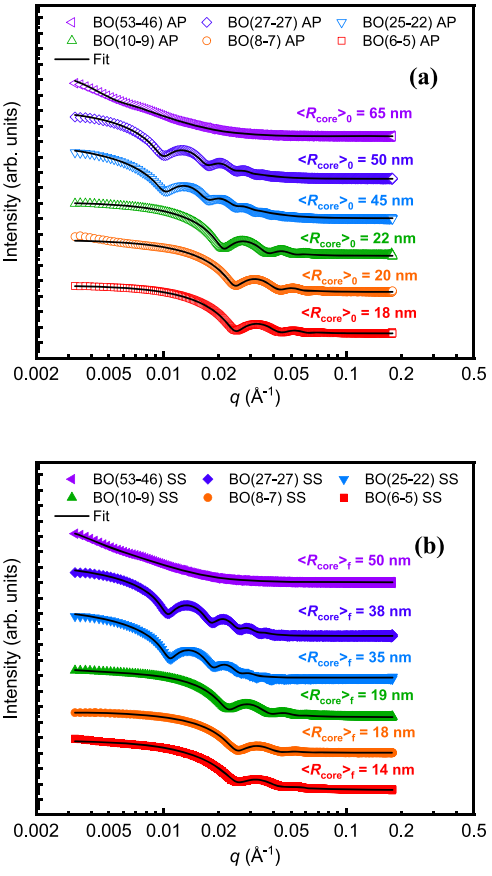

Figure 1. SAXS intensity versus *q*, on logarithmic scales, for 0.25 wt % PB-PEO in $[C_2mim][TFSI]$ (T = 27 °C) (a) as prepared by DD and (b) steady-state after annealing at 170 °C. The black lines represent the best fits of the scattering data to eq 4 with the Pedersen model for block copolymer micelles. The data sets are shifted vertically for clarity.

As with the total micelle radius, $\langle R_{core} \rangle$ from SAXS was found to increase monotonically with *M* for the as-prepared and steady-state micelles, as shown in Figure 2. The changes in micelle size before and after annealing at 170 °C are summarized in Table 2. The percent decrease in $\langle R_{core} \rangle$ exhibits a similar trend to that observed in $\langle R_h \rangle$; the percent decrease in $\langle R_{core} \rangle$ with increasing *M* was 22%, 20%, 14%, 22%, 24%, and 23%. From $\langle R_{core} \rangle$, the average aggregation number *Q* was calculated assuming that the micelle core is devoid of solvent (i.e., $Q = (4\pi\langle R_{core}\rangle^3)/3V_{core}$, where $V_{core} = M_{n,PB}/\rho_{PB}N_{Av}$ is the molar volume of one core block). This is a reasonable approximation for such a strongly segregated system. From these values, the fragmentation process results in a population of micelles with an average aggregation number that is approximately have that of the initial aggregation number. The core size of strongly segregated block copolymer micelles should scale as $R_{core} \sim N_{core}^{3/5}$.[61−63] As shown in Figure 2, $\langle R_{core} \rangle$ increases with N_{core} essentially as predicted for both the as-prepared and steady-state samples. This former result is somewhat unexpected, in that micelles prepared by DD apparently adhere to an equilibrium scaling relationship of $\langle R_{core} \rangle$ with N_{core}, even though they are clearly far from equilibrium. This result highlights another difficulty in assessing the true equilibrium state in block copolymer micelles−apparent adherence to an equilibrium scaling law is far from a sufficient criterion.

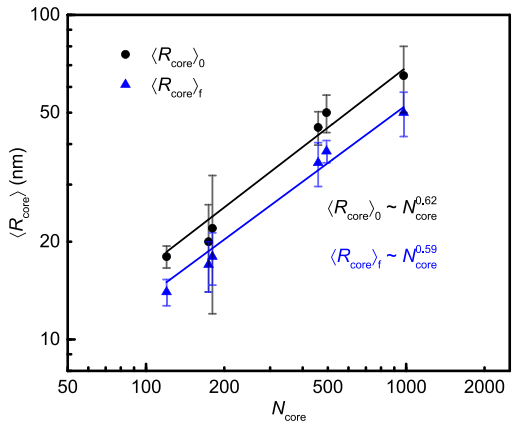

Figure 2. Scaling of $\langle R_{core} \rangle$ versus N_{core} for 0.25 wt % PB-PEO in $[C_2mim][TFSI]$ as prepared by DD (black circles) and steady-state after annealing at 170 °C (blue triangles). The solid lines for the as prepared and steady-state values represent the scaling obtained for $\langle R_{core}\rangle_0 \sim N_{core}^{0.62}$ (black line) and $\langle R_{core}\rangle_f \sim N_{core}^{0.59}$ (blue line). The error bars represent ± σ_{core} shown in Table 2.

Fragmentation Kinetics. The substantial decrease in micelle size after annealing has previously been established as being due to equilibration via micelle fragmentation.[36,45] Thus,

https://doi.org/10.1021/jacs.1c02147
J. Am. Chem. Soc. XXXX, XXX, XXX−XXX

Table 2. Micelle Dimensions for 0.25 wt % Solutions in $[C_2mim][TFSI]$ at T = 27 °C, Before and After Annealing at 170 °C

as prepared by direct dissolution							
sample	$\langle R_h\rangle_0$ (nm)	$\langle \mu_2/\Gamma^2 \rangle_0$	$\langle R_{core}\rangle_0$ (nm)	$\sigma_{core,0}$ (nm)	Q_0[a]	$s_{core,0}$[b]	$s_{corona,0}$[c]
BO(6−5)	29	0.084	18	1.4	1260	2.05	2.22
BO(8−7)	42	0.251	20	6.0	1900	2.45	2.50
BO(10−9)	51	0.229	22	10.0	2400	2.38	3.31
BO(25−22)	70	0.086	45	5.3	8060	2.93	1.86
BO(27−27)	83	0.166	50	6.6	11000	3.38	2.20
BO(53−46)	108	0.177	65	15.0	11400	3.15	2.07
steady-state after annealing at 170 °C							
sample	$\langle R_h\rangle_f$ (nm)	$\langle \mu_2/\Gamma^2 \rangle_f$	$\langle R_{core}\rangle_f$ (nm)	$\sigma_{core,f}$ (nm)	Q_f[a]	$s_{core,f}$[b]	$s_{corona,f}$[c]
BO(6−5)	20	0.050	14	1.3	930	1.97	0.78
BO(8−7)	27	0.050	16	3.0	950	1.60	1.51
BO(10−9)	34	0.042	19	3.3	1500	2.05	1.71
BO(25−22)	58	0.072	35	5.4	3800	2.28	1.72
BO(27−27)	62	0.085	38	3.0	4900	2.57	1.60
BO(53−46)	77	0.085	50	7.8	5200	1.96	1.80

[a]The aggregation number (Q), where the subscripts 0 and f denote initial and final values, respectively, was calculated as $4\pi\langle R_{core}\rangle^3/(3V_{PB})$ assuming the core is devoid of solvent, and $V_{PB} = M_{n,PB}/\rho_{PB}N_{Av}$ is the volume per core chain, ρ_{PB} = 0.89 g/cm^3, N_{Av} is Avogadro's number, and $M_{n,PB}$ is the molecular weight of PB, asreported in Table 1. [b]The degree of core chain stretching (s_{core}), was calculated as $\langle R_{core}\rangle$ divided by the root-mean-square end-to-end distance of the core block using the statistical segment length of PB, b = 5.9 Å.[64] [c]The degree of corona chain stretching (s_{corona}) calculated as the corona thickness ($L_{corona} = \langle R_h\rangle - \langle R_{core}\rangle$) divided by the root-mean-square end-to-end distance of the corona block using the statistical segment length of PEO, b = 6.0 Å.[65]

the fragmentation kinetics were studied for six molecular weights of PB-PEO in $[C_2mim][TFSI]$ using T-jump DLS and TR-SAXS to determine the dependence of the fragmentation time τ on the total degree of polymerization of the copolymer N_{total}. The change in $\langle R_{core}\rangle$ was monitored with high temporal resolution by heating micelle solutions directly on the beamline to 170 °C under vacuum, and the scattering was measured during annealing for 48 h. Representative TR-SAXS data for 0.25 wt % BO(27−27) in $[C_2mim][TFSI]$ are shown in Figure 3, where the background-subtracted intensity traces versus q are plotted as a function of annealing time. Analogous TR-SAXS data for BO(8−7), BO(10−9), and BO(25−22) are provided in the SI, Figures S6−S8.

As shown in Figure 3b, the form factor for BO(27−27) shows a first minimum at q_{min} = 0.009 Å^{-1} after annealing at 170 °C for approximately 26 min, which corresponds to $\langle R_{core}\rangle$ = 50 nm from the hard sphere approximation where qR_{core} = 4.493. Throughout the course of an annealing experiment, the q-position of the first minimum shifts progressively to higher values of q, indicative of a smaller $\langle R_{core}\rangle$. After annealing at 170 °C for approximately 2500 min, q_{min} shifts to 0.012 Å^{-1} and $\langle R_{core}\rangle$ = 37.4 nm. Fitting the scattering data to the block copolymer micelle model before and after annealing at 170 °C shows good agreement with the hard sphere approach used to determine $\langle R_{core}\rangle$ from TR-SAXS.

To quantify the fragmentation kinetics, the change in micelle size, either $\langle R_h\rangle$ or $\langle R_{core}\rangle$, is normalized according to the following:eq 4:

$$R(t) = \frac{\langle R_i\rangle_t - \langle R_i\rangle_f}{\langle R_i\rangle_0 - \langle R_i\rangle_f} = \exp[-(t/\tau)^n] \quad (4)$$

where $R(t)$ is the normalized relaxation function, and i = h or core denotes either the average hydrodynamic radius from DLS or the average micelle core radius from SAXS. The normalized change in size was fit to the Avrami equation or "compressed" exponential, shown in eq 4, where τ is the fragmentation time constant and n is the Avrami exponent. The normalized change in $\langle R_h\rangle$ from DLS is shown in Figure 4, and that for $\langle R_{core}\rangle$ in Figure 5.

From DLS, the change in $\langle R_h\rangle$ while annealing at 170 °C is well-described by eq 4, with an exponent of 2.0−2.3. The fitting was performed using n as an adjustable parameter, resulting in an average value of $n = 2.2 \pm 0.3$. Refitting the data with a fixed exponent of n = 2.0 resulted in fits of similar quality with only modest variations in τ, as shown in Table S1. Attempts to fit the change in normalized $\langle R_h\rangle$ to a single or a double exponential resulted in poor fit quality for the former, and physically unreasonable values of τ for the latter. This is consistent with previous reports on a single, low molecular weight of PB-PEO in various ionic liquids.[36,40,45] From Figure 4, the fragmentation time τ increases strongly with increasing M; the 11 kg mol^{-1} diblock has a τ on the order of 100 min, whereas the 100 kg mol^{-1} diblock has $\tau \approx$ 5000 min. To corroborate the results from T-jump DLS, the time-dependent change in R_{core} from SAXS at 170 °C was normalized according to eq 4. The results for all polymers except BO(53−46) are shown in Figure 5. The dispersity in R_{core} for BO(53−46) made estimating the radius using the hard sphere approximation based on the first minimum of the form factor unreliable. Although the intensity traces for BO(53−46) could be fit to the Pedersen model, the error in $\langle R_{core}\rangle$ was quite large. The large micelle size dispersity and exponent by DLS shown in Table 3 for BO(53−46) are likely due to the fact that this sample is prepared using the same dissolution time as the lower M samples. Due to this uncertainty, the fragmentation kinetics were determined only for the other five M. In general, values of τ obtained from DLS and SAXS agree remarkably well. The fitting results for both experiments are summarized in Table 3.

Molecular Weight Dependence of Fragmentation Time. As noted above, the fragmentation kinetics for PB-PEO in $[C_2mim][TFSI]$ depend strongly on M. Figure 6 shows the values of τ obtained from fitting the normalized change in micelle size to eq 4 as a function of the total degree of polymerization; the results from DLS and SAXS are very

https://doi.org/10.1021/jacs.1c02147
J. Am. Chem. Soc. XXXX, XXX, XXX−XXX

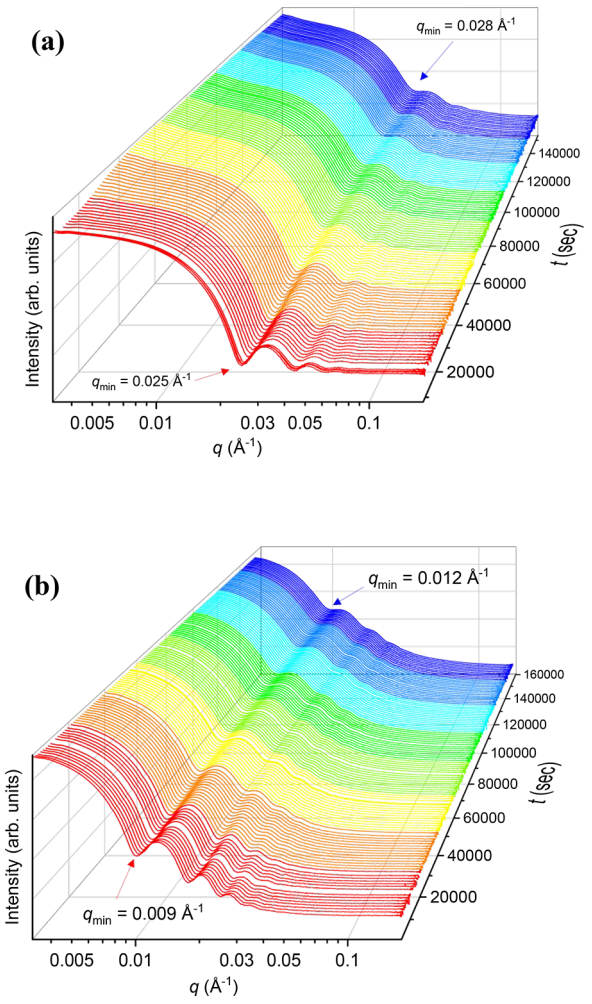

Figure 3. TR-SAXS intensity (logarithmic scale) as a function of q showing the evolution in the micelle core radius while annealing at 170 °C for 0.25 wt % (a) BO(6−5) in [C_2mim][TFSI]. The position of the first minimum in the form factor increases from q_{min} = 0.025 Å^{-1} for short annealing times to q_{min} = 0.028 Å^{-1} at longer annealing times. (b) BO(27−27) in [C_2mim][TFSI]. The first minimum in the form factor increases from q_{min} = 0.009 Å^{-1} at short times to q_{min} = 0.012 Å^{-1} at longer annealing times. The PB core radius can be estimated assuming a hard sphere ($R_{core} \cong 4.493/q_{min}$), so the radius of the micelle core decreases with increasing annealing time.

consistent. The fit to a power law gives the scaling $\tau \sim N_{total}^{1.8\pm0.1}$. Dormidontova proposed a scaling model for micelle fusion kinetics, and further assumed that fragmentation would proceed as the reverse of micelle fusion, and thus the N scaling would be the same for both processes.[27] For micelles with large aggregation numbers (Q) with respect to their equilibrium size, Dormidontova defined a characteristic time for corona deformation (τ_{def}) as the inverse translational diffusion constant for chains, where V_B is the molar volume per monomer unit in the corona.[27]

$$\tau_{def} \cong \frac{\eta_s V_B}{k_B T} N_{corona}^{9/5} Q^{13/5} \quad (5)$$

Assuming the fragmenting micelle is large, Dormidontova's theory proposes that $\tau \sim N_{corona}^{1.8}$ at constant Q, as shown in eq 5. It should be noted that for very large aggregation numbers, such as the ones obtained for the as-prepared micelles, that there is at most a small molecular weight

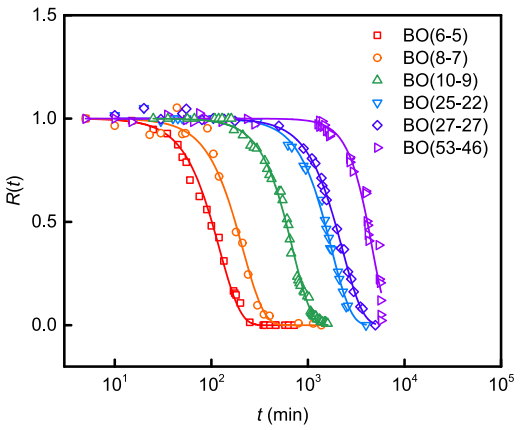

Figure 4. Time dependence of normalized $\langle R_h \rangle$ for 0.25 wt % solutions of BO molecular weight series in [C_2mim][TFSI]. DLS measurements were performed at a scattering angle of 90° and a relaxation temperature of 170 °C. Solid lines represent best fits to eq 4 with n = 2.2 ± 0.3.

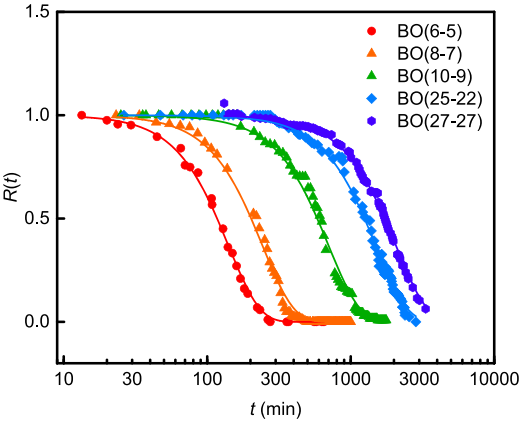

Figure 5. Time dependence of normalized $\langle R_{core} \rangle$ for 0.25 wt % solutions of PB-PEO in [C_2mim][TFSI]. TR-SAXS measurements were performed at a relaxation temperature of 170 °C. Solid lines represent best fits to eq 4 with n = 2.0 ± 0.1.

Table 3. Molecular Weight Dependence of τ Determined by *T*-Jump DLS and TR-SAXS at 170 °C for 0.25 wt % BO in [C_2mim][TFSI]

	T-jump DLS		TR-SAXS	
sample	τ (min)	n	τ (min)	n
BO(6−5)	120 ± 10	2.0	140	2.1
BO(8−7)	200 ± 75	2.0	250	2.2
BO(10−9)	690 ± 90	2.2	710	2.2
BO(25−22)	1750 ± 170	2.2	1500	2.1
BO(27−27)	2300 ± 250	2.1	2070	2.3
BO(53−46)	5000 ± 360	2.7		

dependence to Q. The Q dependence of τ is shown in the SI, where $\tau \sim Q_0^{1.7\pm0.1}$. The agreement between the scaling of τ with N_{corona} and Q_0 implies that the strong Q dependence from eq 5 does not reflect our experimental results, and this is consistent with the assumption that Q does not depend strongly on N_{total} for very large Q.

The results are apparently in excellent agreement with the theory. However, some caution is warranted. First, the theory does not anticipate the compressed exponential form in eq 4, so there is clearly an aspect of the fragmentation mechanism

https://doi.org/10.1021/jacs.1c02147
J. Am. Chem. Soc. XXXX, XXX, XXX−XXX

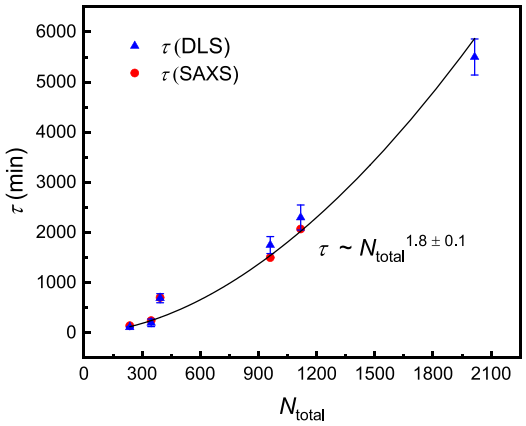

Figure 6. Dependence of the fragmentation time constants (τ) determined by T-jump DLS (red circles) and TR-SAXS (blue triangles) on the degree of polymerization of PEO (N_{PEO}).

that is not yet fully appreciated. Second, the separate effects of N_{core} and N_{corona} on the experimental fragmentation times cannot be assessed individually because the volume fraction of PEO in this work has been constant. Thus, the experimental scaling represents the dependence of the fragmentation time on the total degree of polymerization, which may not coincide with the dependence on N_{corona}. However, it does seem physically reasonable that the corona plays a much larger role in the process than the core. Further discussion of the time constants from the model and from estimates of corona dynamics are provided in the SI.

To rationalize the dependence of the fragmentation kinetics on molecular weight, one must consider the transition state and activation barrier of this process. Previous work on this system revealed that the fragmentation kinetics were unaffected by changes in the solvent selectivity toward the core-forming block,[45] thus indicating independence of interfacial tension. Accordingly, we propose that severe corona crowding in the transition state is the primary barrier to fragmentation. When considering the free energy of polymer chains in a block copolymer micelle at equilibrium, the interfacial free energy and the free energy of chains in the corona contribute more to the total free energy of the micelle compared to the free energy of chains in the core.[12,61,66] We calculate the free energy of PB-PEO micelles as prepared by DD, after annealing at 170 °C, and for the proposed "peanut-shaped" transition state (Figure S10) observed in previous work on PB−PEO in [C_2mim][TFSI] by high-temperature liquid phase transmission electron microscopy.[46] A schematic illustration of the transition state is shown in Figure S11. The total free energy of a spherical block copolymer micelle in solution (F_{mic}) was well described by Zhulina et al.,[12] and is given by the sum of the free energy contribution from the core chains (F_{core}), the free energy of the corona chains (F_{corona}), and the interfacial energy (F_{int}). Therefore, the free energy can be estimated for the as-prepared and steady state micelles. Some details on this calculation are provided in the SI, and were previously reported by Zhulina et al.[12] Because the transition state morphology is "peanut-shaped" the transition state free energy cannot be treated in the same manner as the spherical micelles before and after fragmentation. The calculated free energies are reported in Table S4.

To calculate the corona free energy in the transition state, the fraction of corona chains overlapped in the neck region must be estimated. The transition state is represented schematically in Figure S11. We propose that the increase in the local concentration of corona chains near the neck point, i.e., the increase in the number of blobs per corona chain n_{blob}, in the formation of the transition state is the primary barrier to fragmentation. To estimate the degree of corona crowding in the transition state first, we estimate the fraction of corona overlap in the transition state, and then relate the overlap fraction to the concentration of blobs per PEO chain in the neck region using the theory from Zhulina et al.[12] Using a simplified model for the transition state, illustrated in Figure S12, to determine the area of corona overlap in the transition state results in approximately 1/6 of the corona chains overlapping for all molecular weights. Details on this calculation are provided in the SI. Then, the concentration of PEO chains in the neck region of the transition state is determined by estimating the number of blobs per corona chain. In the neck region, the number of blobs per chain is expected to be approximately twice the number of blobs per chain in the as-prepared micelles ($n_{blob,neck} = 2n_{blob,sphere} = 2F_{corona,0}/k_BT$), whereas the outer spherical regions would have $n_{blob,sphere} = F_{corona,0}/k_BT$, where the free energy is calculated using the as-prepared size of the micelle as shown in eq S11.

The transition state free energy for the core and the interface was calculated using the steady state micelle dimensions. The transition state corona free energy was calculated assuming 5/6 of the chains are described by $F_{corona,0}/k_BT$, and for the 1/6 of corona chains overlapped in the neck region, the corona free energy is $2F_{corona,0}$. Therefore, the total corona free energy in the transition state is calculated as $F_{corona,TS}/k_BT = (5/6)F_{corona,0}/k_BT + (1/3)F_{corona,0}/k_BT$. Details on this calculation are provided in the SI. From Table S4, the average n_{blob} is 16 for BO(53−46) before a T-jump to 170 °C. Assuming that the number of blobs in the neck point is double the calculated $n_{blob,0}$ shown in Table S4, approximately 1/6 of the corona chains experience corona crowding where there are approximately 32 blobs per chain near the neck, whereas n_{blob} is 16 for chains in the spherical region of the micelle indicated in Figure S11. The fraction of corona chain overlap was determined to be 1/6 for all molecular weights by eq S8, and thus n_{blob} at the neck point is 8, 9, 10, 21, 24, and 32 for BO(6−5), BO (8−7), BO(10−9), BO(25−22), BO(27−27), and BO(53−46). This large increase in the local concentration of PEO chains in the neck region of the transition state supports the strong molecular weight dependence of micelle fragmentation kinetics. Because the confinement free energy of corona chains is directly proportional to n_{blob}, the chains near the neck point become much more confined and the entropic penalty associated with this chain confinement contributes to this being the primary activation barrier to fragmentation.

Although these estimates are encouraging, we emphasize that the uncertainties in estimating the transition state free energy are quite large, and the differences in the calculated free energies for the spherical and "peanut" shaped micelles are only ~5−10k_BT. Given that the aggregation numbers are huge and the barrier is known to be of order 30−40 kT,[36,45] the estimated barriers per chain are small fractions of kT, and beyond the resolution of this calculation.

Molecular Weight Dependence of Initial Micelle Size by Direct Dissolution. To understand the N dependence of the initial core size for micelles prepared by DD, SAXS measurements on the pure PB−PEO diblock copolymers were conducted. The 1D scattering intensity traces for these

https://doi.org/10.1021/jacs.1c02147
J. Am. Chem. Soc. XXXX, XXX, XXX−XXX

samples are shown in Figure S9. It has been suggested that the morphology of micelles prepared by direct dissolution depends on the morphology of the bulk diblock copolymer.[36,67] The scattering data confirms that BO(6−5), BO(8−7), BO(10−9), BO(25−22), and BO(27−27) exhibit a lamellar morphology at 70 °C, which is the temperature used for preparing micelle solutions by direct dissolution. The domain size of the PB lamellae was estimated from the q-position of the primary scattering peak ($d = 2\pi/q^*$) and the known volume fraction of PB. The domain sizes were found to be approximately 16, 17, 19, 47, and 54 nm for BO(6−5), BO(8−7), BO(10−9), BO(25−22), and BO(27−27), respectively. Interestingly, the domain sizes obtained from SAXS of the bulk polymers are comparable to the initial micelle core size. This dependence is represented in Figure 7 as a plot of $\langle R_{core}\rangle_0$ vs d_{PB}. From this

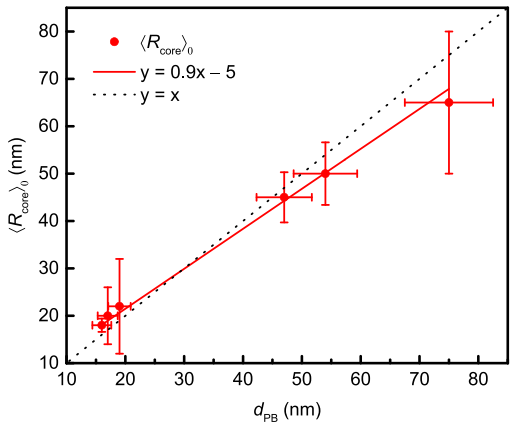

Figure 7. Dependence of $\langle R_{core}\rangle_0$ (nm) on the PB domain size (d_{PB}) indicating a direct relationship between $\langle R_{core}\rangle_0$ for micelles prepared by DD and the PB domain size of the bulk diblock copolymer. The solid red line represents the best linear fit to $\langle R_{core}\rangle_0$ as a function of d_{PB}, and the dotted black line represents $y = x$. The error bars in $\langle R_{core}\rangle_0$ represent ± σ_{core} from Table 2, and 10% error in d_{PB} is assumed.

figure, the direct relationship between the domain size of the bulk copolymer and the initial micelle core radius is apparent. This result is also consistent with the previous reports on BO(8−7) in 1-alkyl-3-methylimidazolium bis-(trifluoromethylsulfonyl)imide-based ionic liquids.[36,45]

It should be noted that a linear dependence should not necessarily be expected. The dependence begins to weaken slightly at higher molecular weights, as evidenced by the slight downward curvature of $\langle R_{core}\rangle$ for the two largest polymers. The dependence of $\langle R_{core}\rangle_0$ on d_{PB} follows the strong segregation limit scaling of 2/3,[68] as shown in Figure S13, while the apparent equilibrium scaling of $\langle R_{core}\rangle$ with N_{core} for the initial micelles has an exponent closer to 3/5, as shown in Figure 2. These slightly different dependences give rise to the curvature evident in Figure 7. Figure S13 shows the relationship of d_{PB} as a function of N_{core} for the domain size determined experimentally by SAXS, and the estimated domain spacing calculated from self-consistent field theory (SCFT); the experimental domain size of the PB lamellae agrees well with SCFT. We therefore speculate that during direct dissolution the solvent penetrates the PEO domains, peeling apart layers of PEO-decorated PB layers. Some surface instabilities in these separate layers drive a pinching-off process to give large, disperse spherical aggregates in solution. This behavior is broadly analogous to a Rayleigh instability, and has been referenced in computations of surfactant-based micelles,[69] and experimentally in cylinder-to-sphere transitions[70−75] in block copolymer micelles. In experimental works on the cylinder-to-sphere transitions in block copolymer micelles, it is concluded that the surface-instability-mediated transitions induce pinching of immature spherical micelles, followed by rapid chain exchange.[74] On the basis of the lack of chain exchange in BO/[C_2mim][TFSI] systems reported previously,[36] the direct dissolution mechanism is related to this process, but not identical. Furthermore, even accounting for the molar mass difference, our system undergoes fragmentation about 3 orders of magnitude slower than the PEP-PEO cylindrical micelles, implying a very small barrier in the latter case.

Another possibly surprising result of the dependence of $\langle R_{core}\rangle_0$ on d_{PB} is that the micelles prepared by direct dissolution have a core radius that is approximately equal to the full PB domain size, rather than $d_{PB}/2$. The interfacial tension in the swollen state is clearly greater than in the dry copolymer, so an increase in core chain stretching is certainly expected. Moreover, the degree of interdigitation of the PB chains in the dry lamellae can affect this picture of the dissolution mechanism. In the dry state, the degree of stretching of PB (s_{PB}) can be estimated from two limits: the first assumes no interdigitation of chains, where $s_{PB,1} = d_{PB}/\langle h^2\rangle_0^{1/2}$; the second method assumes full interdigitation of chains, where $s_{PB,2} = d_{PB}/2\langle h^2\rangle_0^{1/2}$. Calculating the degree of stretching for BO(8−7) by these two methods gives $s_{PB,1} = 1.1$ and $s_{PB,2} = 2.2$, respectively. These may be to the degree of stretching of chains in the micelle core from Table 2, $s_{core} = 2.5$. This result implies some significant degree of interdigitation in the bulk state.

CONCLUSIONS

In this work, the effect of polymer molecular weight on micelle fragmentation kinetics was studied for the first time, using six molecular weights of PB−PEO with a near constant volume fraction of PEO ($f_{PEO} \approx 0.40$) in the ionic liquid [C_2mim][TFSI]. Disperse micelles prepared by direct dissolution in [C_2mim][TFSI] were found to be larger than the equilibrium size, and all molecular weight micelles decreased in size, both $\langle R_h\rangle$ and $\langle R_{core}\rangle$, when subjected to high temperature annealing. The decrease in micelle size while annealing at 170 °C was monitored by T-jump DLS and TR-SAXS, and it was concluded that PB-PEO micelles equilibrate by fragmentation. The final aggregation number was approximately half of the original aggregation number prior to a T-jump. The decay in $\langle R_h\rangle$ and $\langle R_{core}\rangle$ was consistently well described by a compressed exponential with an exponent of 2; the origin of this functional form remains to be elucidated. The characteristic fragmentation times determined by fitting the normalized change in micelle size to this equation was found to depend strongly on the molecular weight of the block copolymer, where $\tau \sim N_{total}^{1.8 \pm 0.1}$. A previous model of micelle fragmentation by Dormidontova predicts a similar scaling, albeit in terms of N_{corona}. Future measurements on a series of polymers with constant N_{core} will be required to assess whether this apparent agreement is robust. The core size of the initial micelles was shown to correlate closely with the PB domain dimensions in the precursor dry, lamellar copolymer, suggesting a formation mechanism involving peeling apart of layers, followed by pinching off into spherical domains.

https://doi.org/10.1021/jacs.1c02147
J. Am. Chem. Soc. XXXX, XXX, XXX−XXX

■ ASSOCIATED CONTENT

Supporting Information

The Supporting Information is available free of charge at https://pubs.acs.org/doi/10.1021/jacs.1c02147.

SEC-RI traces of PB-PEO diblocks, ^{1}H NMR spectra of PB−PEO diblocks and [C_2mim][TFSI], REPES results for PB−PEO in [C_2mim][TFSI] as-prepared by DD and steady-state after annealing, dependence of $\langle R_h \rangle$ on the total degree of polymerization N_{total} for 0.25 wt % PB-PEO in [C_2mim][TFSI], fragmentation times with fixed n, TR-SAXS traces for BO(8−7), BO(10−9), and BO(25−22), calculations of corona chain disentanglement time, SAXS of bulk PB−PEO, high temperature liquid-phase transmission electron microscopy of BO(53−46) in [C_2mim][TFSI], calculations of the fraction of corona overlap in the transition state, high temperature LP-TEM micrograph of BO(53−46) in [C_2mim][TFSI] at 170 °C, schematic illustration of fragmentation transition state, illustration of simplified model transition state for calculating corona chain overlap, calculation of micelle free energy, domain spacing from SAXS of of BO(x−y) diblock copolymers in the bulk, Comparison of the domain size of PB determined by SAXS and the estimated domain size for a lamellar diblock copolymer using self-consistent field theory, estimated fragmentation lag time as a function of degree of polymerization, and dependence of fragmentation time on as-prepared aggregation number (PDF)

■ AUTHOR INFORMATION

Corresponding Author

Timothy P. Lodge − *Department of Chemical Engineering and Materials Science and Department of Chemistry, University of Minnesota, Minneapolis, Minnesota 55455-0431, United States;* orcid.org/0000-0001-5916-8834; Email: lodge@umn.edu

Authors

Julia T. Early − *Department of Chemistry, University of Minnesota, Minneapolis, Minnesota 55455-0431, United States; Center for Functional Nanomaterials, Brookhaven National Laboratory, Upton, New York 11973-5000, United States;* orcid.org/0000-0002-5794-7161

Alison Block − *Department of Chemical Engineering and Materials Science, University of Minnesota, Minneapolis, Minnesota 55455-0431, United States*

Kevin G. Yager − *Center for Functional Nanomaterials, Brookhaven National Laboratory, Upton, New York 11973-5000, United States;* orcid.org/0000-0001-7745-2513

Complete contact information is available at: https://pubs.acs.org/10.1021/jacs.1c02147

Notes

The authors declare no competing financial interest.

■ ACKNOWLEDGMENTS

This work was supported primarily by the National Science Foundation (DMR-1707578). Additional support came from the University of Minnesota Doctoral Dissertation Fellowship (JTE), the University of Minnesota Robert and Jill DeMaster Excellence Fellowship (J.T.E.), the Research Experiences for Undergraduates (REU) Program of the National Science Foundation under Award Number DMR-1559833 (through the University of Minnesota MRSEC under Award Number DMR-2011401, A.B.), and from the U.S. Department of Energy (DOE), Office of Science, Office of Workforce Development for Teachers and Scientists, Office of Science Graduate Student Research (SCGSR) program (J.T.E.). The SCGSR program is administered by the Oak Ridge Institute for Science and Education (ORISE) for the DOE. ORISE is managed by ORAU under contract number DE-SC0014664. Portions of this work were performed at the Center for Functional Nanomaterials, and the National Synchrotron Light Source II, Brookhaven National Laboratory, which are supported by the U.S. DOE Office of Science under Contract DE-SC0012704. Portions of this work were performed at the DuPont-Northwestern-Dow Collaborative Access Team (DND-CAT) located at Sector 5 of the Advanced Photon Source (APS). DND-CAT is supported by Northwestern University, E.I. DuPont de Nemours & Co., and The Dow Chemical Company. This research used resources of the Advanced Photon Source, a U.S. Department of Energy (DOE) Office of Science User Facility operated for the DOE Office of Science by Argonne National Laboratory under Contract No. DE-AC02-06CH11357. We thank Dr. Ruipeng Li and Dr. Esther Tsai for assistance with TR-SAXS measurements at the 11-BM CMS beamline at the NSLS-II and Dr. Lihua Zhang for insightful discussions on high temperature LP-TEM. We thank Claire Seitzinger for assisting with SAXS measurements of bulk PB-PEO diblocks.

■ REFERENCES

(1) Tang, B.; White, S. P.; Frisbie, C. D.; Lodge, T. P. Synergistic Increase in Ionic Conductivity and Modulus of Triblock Copolymer Ion Gels. *Macromolecules* **2015**, *48*, 4942−4950.

(2) Tang, B.; Schneiderman, D. K.; Zare Bidoky, F.; Frisbie, C. D.; Lodge, T. P. Printable, Degradable, and Biocompatible Ion Gels from a Renewable ABA Triblock Polyester and a Low Toxicity Ionic Liquid. *ACS Macro Lett.* **2017**, *6*, 1083−1088.

(3) Kataoka, K.; Harada, A.; Nagasaki, Y. Block Copolymer Micelles for Drug Delivery: Design, Characterization and Biological Significance. *Adv. Drug Delivery Rev.* **2012**, *64*, 37−48.

(4) Li, Z.; Johnson, L. M.; Ricarte, R. G.; Yao, L. J.; Hillmyer, M. A.; Bates, F. S.; Lodge, T. P. Enhanced Performance of Blended Polymer Excipients in Delivering a Hydrophobic Drug through the Synergistic Action of Micelles and HPMCAS. *Langmuir* **2017**, *33*, 2837−2848.

(5) Cotanda, P.; Lu, A.; Patterson, J. P.; Petzetakis, N.; O'Reilly, R. K. Functionalized Organocatalytic Nanoreactors: Hydrophobic Pockets for Acylation Reactions in Water. *Macromolecules* **2012**, *45*, 2377−2384.

(6) Anderson, W. Block Copolymers as Viscosity Index Improvers for Lubrication Oils. US 3763044, 1973.

(7) Zhao, D.; Ma, Y.; Lodge, T. P. Exchange Kinetics for a Single Block Copolymer in Micelles of Two Different Sizes. *Macromolecules* **2018**, *51*, 2312−2320.

(8) Zinn, T.; Willner, L.; Pipich, V.; Richter, D.; Lund, R. Molecular Exchange Kinetics of Micelles: Corona Chain Length Dependence. *ACS Macro Lett.* **2016**, *5*, 884−888.

(9) Ma, Y.; Lodge, T. P. Chain Exchange Kinetics in Diblock Copolymer Micelles in Ionic Liquids: The Role of χ. *Macromolecules* **2016**, *49*, 9542−9552.

(10) Denkova, A. G.; Mendes, E.; Coppens, M.-O. Non-Equilibrium Dynamics of Block Copolymer Micelles in Solution: Recent Insights and Open Questions. *Soft Matter* **2010**, *6*, 2351.

(11) Halperin, A.; Tirrell, M.; Lodge, T. P. Tethered Chains in Polymer Microstructures. *Macromol. Synth. Order Adv. Prop.* **1992**, *100* (1), 31−71.

(12) Zhulina, E. B.; Adam, M.; Larue, I.; Sheiko, S. S.; Rubinstein, M. Diblock Copolymer Micelles in a Dilute Solution. *Macromolecules* **2005**, *38*, 5330−5351.
(13) He, Y.; Li, Z.; Simone, P.; Lodge, T. P. Self-Assembly of Block Copolymer Micelles in an Ionic Liquid. *J. Am. Chem. Soc.* **2006**, *128*, 2745−2750.
(14) Choi, S.; Bates, F. S.; Lodge, T. P. Structure of Poly (Styrene-b-Ethylene-Alt-Propylene) Diblock Copolymer Micelles in Squalane. *J. Phys. Chem. B* **2009**, *113*, 13840−13848.
(15) Wang, E.; Lu, J.; Bates, F. S.; Lodge, T. P. Effect of Corona Block Length on the Structure and Chain Exchange Kinetics of Block Copolymer Micelles. *Macromolecules* **2018**, *51*, 3563−3571.
(16) Yu, K.; Zhang, L.; Eisenberg, A. Novel Morphologies of "Crew-Cut" Aggregates of Amphiphilic Diblock Copolymers in Dilute Solution. *Langmuir* **1996**, *12*, 5980−5984.
(17) Bang, J.; Jain, S.; Li, Z.; Lodge, T. P.; Pedersen, J. S.; Kesselman, E.; Talmon, Y. Sphere, Cylinder, and Vesicle Nanoaggregates in Poly(Styrene-b-Isoprene) Diblock Copolymer Solutions. *Macromolecules* **2006**, *39*, 1199−1208.
(18) Aniansson, E. A. G.; Wall, S. N. On the Kinetics of Step-Wise Micelle Association. *J. Phys. Chem.* **1974**, *78*, 1024−1030.
(19) Aniansson, E. A. G.; Wall, S. N.; Almgren, M.; Hoffmann, H.; Kielmann, I.; Ulbricht, W.; Zana, R.; Lang, J.; Tondre, C. Theory of the Kinetics of Micellar Equilibria and Quantitative Interpretation of Chemical Relaxation Studies of Micellar Solutions of Ionic Surfactants. *J. Phys. Chem.* **1976**, *80*, 905−922.
(20) Rharbi, Y.; Winnik, M. A.; Hahn, K. G. Kinetics of Fusion and Fragmentation Nonionic Micelles: Triton X-100. *Langmuir* **1999**, *15* (14), 4697−4700.
(21) Goldmints, I.; Holzwarth, J. F.; Smith, K. a.; Hatton, T. A. Micellar Dynamics in Aqueous Solutions of PEO-PPO-PEO Block Copolymers †. *Langmuir* **1997**, *13*, 6130−6134.
(22) Rharbi, Y. Fusion and Fragmentation Dynamics at Equilibrium in Triblock Copolymer Micelles. *Macromolecules* **2012**, *45*, 9823−9826.
(23) Rharbi, Y.; Karrouch, M.; Richardson, P. Fusion and Fission Inhibited by the Same Mechanism in Electrostatically Charged Surfactant Micelles. *Langmuir* **2014**, *30*, 7947−7952.
(24) Michels, B.; Waton, G.; Zana, R. Dynamics of Micelles of Poly (Ethylene Oxide) - Poly (Propylene Oxide) - Poly (Ethylene Oxide) Block Copolymers in Aqueous Solutions. *Langmuir* **1997**, *13* (12), 3111−3118.
(25) Halperin, A.; Alexander, S. Polymeric Micelles: Their Relaxation Kinetics. *Macromolecules* **1989**, *22*, 2403−2412.
(26) Halperin, A. On Micellar Exchange: The Role of the Insertion Penalty. *Macromolecules* **2011**, *44*, 5072−5074.
(27) Dormidontova, E. E. Micellization Kinetics in Block Copolymer Solutions: Scaling Model. *Macromolecules* **1999**, *32*, 7630−7644.
(28) Nyrkova, I. A.; Semenov, A. N. On the Theory of Micellization Kinetics. *Macromol. Theory Simul.* **2005**, *14*, 569−585.
(29) Lu, J.; Bates, F. S.; Lodge, T. P. Addition of Corona Block Homopolymer Retards Chain Exchange in Solutions of Block Copolymer Micelles. *Macromolecules* **2016**, *49*, 1405−1413.
(30) Lu, J.; Bates, F. S.; Lodge, T. P. Chain Exchange in Binary Copolymer Micelles at Equilibrium: Confirmation of the Independent Chain Hypothesis. *ACS Macro Lett.* **2013**, *2*, 451−455.
(31) Lu, J.; Bates, F. S.; Lodge, T. P. Remarkable Effect of Molecular Architecture on Chain Exchange in Triblock Copolymer Micelles. *Macromolecules* **2015**, *48*, 2667−2676.
(32) Willner, L.; Poppe, A.; Allgaier, J.; Monkenbusch, M.; Richter, D. Time-Resolved SANS for the Determination of Unimer Exchange Kinetics in Block Copolymer Micelles. *Europhys. Lett.* **2001**, *55*, 667−673.
(33) Lund, R.; Willner, L.; Stellbrink, J.; Lindner, P.; Richter, D. Logarithmic Chain-Exchange Kinetics of Diblock Copolymer Micelles. *Phys. Rev. Lett.* **2006**, *96* (6), 1−4.
(34) Lund, R.; Willner, L.; Richter, D.; Dormidontova, E. E. Equilibrium Chain Exchange Kinetics of Diblock Copolymer Micelles: Tuning and Logarithmic Relaxation. *Macromolecules* **2006**, *39*, 4566−4575.
(35) Lund, R.; Willner, L.; Stellbrink, J.; Richter, D. Equilibrium Exchange Kinetics in PEP-PEO Block Copolymer Micelles. A Time Resolved SANS Study. *Phys. B* **2006**, *385*−*386*, 735−737.
(36) Meli, L.; Santiago, J. M.; Lodge, T. P. Path-Dependent Morphology and Relaxation Kinetics of Highly Amphiphilic Diblock Copolymer Micelles in Ionic Liquids. *Macromolecules* **2010**, *43*, 2018−2027.
(37) Choi, S. H.; Lodge, T. P.; Bates, F. S. Mechanism of Molecular Exchange in Diblock Copolymer Micelles: Hypersensitivity to Core Chain Length. *Phys. Rev. Lett.* **2010**, *104* (4), 1−4.
(38) Zinn, T.; Willner, L.; Lund, R.; Pipich, V.; Richter, D. Equilibrium Exchange Kinetics in N-Alkyl-PEO Polymeric Micelles: Single Exponential Relaxation and Chain Length Dependence. *Soft Matter* **2012**, *8*, 623−626.
(39) Zhang, L.; Eisenberg, A. Thermodynamic vs Kinetic Aspects in the Formation and Morphological Transitions of Crew-Cut Aggregates Produced by Self-Assembly of Polystyrene-b-Poly(Acrylic Acid) Block Copolymers in Dilute Solution. *Macromolecules* **1999**, *32*, 2239−2249.
(40) Meli, L.; Lodge, T. P. Equilibrium vs Metastability: High-Temperature Annealing of Spherical Block Copolymer Micelles in an Ionic Liquid. *Macromolecules* **2009**, *42*, 580−583.
(41) Kelley, E. G.; Murphy, R. P.; Seppala, J. E.; Smart, T. P.; Hann, S. D.; Sullivan, M. O.; Epps, T. H. Size Evolution of Highly Amphiphilic Macromolecular Solution Assemblies via a Distinct Bimodal Pathway. *Nat. Commun.* **2014**, *5*, 3599.
(42) Honda, C.; Hasegawa, Y.; Hirunuma, R.; Nose, T. Micellization Kinetics of Block Copolymers in Selective Solvent. *Macromolecules* **1994**, *27*, 7660−7668.
(43) Honda, C.; Abe, Y.; Nose, T. Relaxation Kinetics of Micellization in Micelle-Forming Block Copolymer in Selective Solvent. *Macromolecules* **1996**, *29*, 6778−6785.
(44) Parent, L. R.; Bakalis, E.; Ramírez-Hernández, A.; Kammeyer, J. K.; Park, C.; De Pablo, J.; Zerbetto, F.; Patterson, J. P.; Gianneschi, N. C. Directly Observing Micelle Fusion and Growth in Solution by Liquid-Cell Transmission Electron Microscopy. *J. Am. Chem. Soc.* **2017**, *139*, 17140−17151.
(45) Early, J. T.; Lodge, T. P. Fragmentation of 1,2-Polybutadiene-Block-Poly(Ethylene Oxide) Micelles in Imidazolium-Based Ionic Liquids. *Macromolecules* **2019**, *52*, 7089−7101.
(46) Early, J. T.; Yager, K. G.; Lodge, T. P. Direct Observation of Micelle Fragmentation via In Situ Liquid- Phase Transmission Electron Microscopy. *ACS Macro Lett.* **2020**, *9*, 756−761.
(47) Zaitsau, D. H.; Kabo, G. J.; Strechan, A. A.; Paulechka, Y. U.; Tschersich, A.; Verevkin, S. P.; Heintz, A. Experimental Vapor Pressures of 1-Alkyl-3-Methylimidazolium Bis-(Trifluoromethylsulfonyl)Imides and a Correlation Scheme for Estimation of Vaporization Enthalpies of Ionic Liquids. *J. Phys. Chem. A* **2006**, *110*, 7303−7306.
(48) Hillmyer, M. A.; Bates, F. S. Synthesis and Characterization of Model Polyalkane-Poly(Ethylene Oxide) Block Copolymers. *Macromolecules* **1996**, *29*, 6994−7002.
(49) Brandrup, J.; Immergut, E. H.; Grulke, E. A. *Polymer Handbook*; Wiley-Interscience: New York, 1999, 1−1102.
(50) Bonhôte, P.; Dias, A.-P.; Papageorgiou, N.; Kalyanasundaram, K.; Grätzel, M. Hydrophobic, Highly Conductive Ambient-Temperature Molten Salts. *Inorg. Chem.* **1996**, *35*, 1168−1178.
(51) Brown, W. *Dynamic Light Scattering: The Method and Some Applications (Monographs on the Physics and Chemistry of Materials)*; Clarendon Press/Oxford University Press: Oxford (England)/New York, 1993, 1−752.
(52) Bai, Z.; He, Y.; Lodge, T. P. Block Copolymer Micelle Shuttles with Tunable Transfer Temperatures between Ionic Liquids and Aqueous Solutions. *Langmuir* **2008**, *24*, 5284−5290.
(53) Tokuda, H.; Hayamizu, K.; Ishii, K.; Susan, M. A. B. H.; Watanabe, M. Physicochemical Properties and Structures of Room

https://doi.org/10.1021/jacs.1c02147
J. Am. Chem. Soc. XXXX, XXX, XXX−XXX

Temperature Ionic Liquids. 1. Variation of Anionic Species. *J. Phys. Chem. B* **2004**, *108*, 16593−16600.
(54) Nazet, A.; Sokolov, S.; Sonnleitner, T.; Makino, T.; Kanakubo, M.; Buchner, R. Densities, Viscosities, and Conductivities of the Imidazolium Ionic Liquids [Emim][Ac], [Emim][FAP], [Bmim]-[BETI], [Bmim][FSI], [Hmim][TFSI], and [Omim][TFSI]. *J. Chem. Eng. Data* **2015**, *60*, 2400−2411.
(55) Zhao, N.; Jacquemin, J.; Oozeerally, R.; Degirmenci, V. New Method for the Estimation of Viscosity of Pure and Mixtures of Ionic Liquids Based on the UNIFAC - VISCO Model. *J. Chem. Eng. Data* **2016**, *61*, 2160−2169.
(56) Jakes, J. (Institute of M. C. Testing of the Constrained Regularization Method of Inverting Laplace Transform on Simulated Very Wide Quasielastic Light Scattering Autocorrelation Functions. *Czech. J. Phys.* **1988**, *38*, 1305−1316.
(57) Kharel, A.; Lodge, T. P. Coil Dimensions of Poly(Ethylene Oxide) in an Ionic Liquid by Small-Angle Neutron Scattering. *Macromolecules* **2017**, *50*, 8739−8744.
(58) Pedersen, J. S.; Svaneborg, C.; Almdal, K.; Hamley, I. W.; Young, R. N. A Small-Angle Neutron and x-Ray Contrast Variation Scattering Study of the Structure of Block Copolymer Micelles: Corona Shape and Excluded Volume Interactions. *Macromolecules* **2003**, *36*, 416−433.
(59) Pedersen, J. S. Determination of Size Distributions from Small-Angle Scattering Data for Systems with Effective Hard-Sphere Interactions. *J. Appl. Crystallogr.* **1994**, *27*, 595−608.
(60) Pedersen, J. S.; Svaneborg, C. Scattering from Block Copolymer Micelles. *Curr. Opin. Colloid Interface Sci.* **2002**, *7*, 158−166.
(61) Halperin, A. Polymeric Micelles: A Star Model. *Macromolecules* **1987**, *20*, 2943−2946.
(62) Ma, Y.; Lodge, T. P. Poly(Methyl Methacrylate)-Block-Poly(n-Butyl Methacrylate) Diblock Copolymer Micelles in an Ionic Liquid: Scaling of Core and Corona Size with Core Block Length. *Macromolecules* **2016**, *49*, 3639−3646.
(63) Nagarajan, R.; Ganesh, K. Block Copolymer Self-Assembly in Selective Solvents: Spherical Micelles with Segregated Cores. *J. Chem. Phys.* **1989**, *90*, 5843−5856.
(64) Bates, F. S. Measurement of the Correlation Hole in Homogeneous Block Copolymer Melts. *Macromolecules* **1985**, *18*, 525−528.
(65) Hiemenz, P. C.; Lodge, T. P. *Polymer Chemistry*, 2nd ed.; Taylor & Francis Group/CRC Press: Boca Raton, 2007, 1−587.
(66) Zhulina, E. B.; Borisov, O. V. Theory of Block Polymer Micelles: Recent Advances and Current Challenges. *Macromolecules* **2012**, *45*, 4429−4440.
(67) Cameron, N. S.; Corbierre, M. K.; Eisenberg, A. 1998 E.W.R. Steacie Award Lecture Asymmetric Amphiphilic Block Copolymers in Solution: A Morphological Wonderland. *Can. J. Chem.* **1999**, *77* (8), 1311−1326.
(68) Helfand, E.; Wasserman, Z. R. Block Copolymer Theory. 4. Narrow Interphase Approximation. *Macromolecules* **1976**, *9*, 879−888.
(69) Sammalkorpi, M.; Karttunen, M.; Haataja, M. Micelle Fission through Surface Instability and Formation of an Interdigitating Stalk. *J. Am. Chem. Soc.* **2008**, *130*, 17977−17980.
(70) Ryu, C. Y.; Vigild, M. E.; Lodge, T. P. Fluctuations with Cubic Symmetry in a Hexagonal Copolymer Microstructure. *Phys. Rev. Lett.* **1998**, *81*, 5354−5357.
(71) Ryu, C. Y.; Lodge, T. P. Thermodynamic Stability and Anisotropie Fluctuations in the Cylinder-to-Sphere Transition of a Block Copolymer. *Macromolecules* **1999**, *32*, 7190−7201.
(72) Burke, S. E.; Eisenberg, A. Kinetics and Mechanisms of the Sphere-to-Rod and Rod-to-Sphere Transitions in the Ternary System PS310-b-PAA52/Dioxane/Water. *Langmuir* **2001**, *17*, 6705−6714.
(73) Abbas, S.; Li, Z.; Hassan, H.; Lodge, T. P. Thermoreversible Morphology Transitions of Poly(Styrene-b-Dimethylsiloxane) Di-block Copolymer Micelles in Dilute Solution. *Macromolecules* **2007**, *40*, 4048−4052.
(74) Lund, R.; Willner, L.; Richter, D.; Lindner, P.; Narayanan, T. Kinetic Pathway of the Cylinder-to-Sphere Transition in Block Copolymer Micelles Observed in Situ by Time-Resolved Neutron and Synchrotron Scattering. *ACS Macro Lett.* **2013**, *2*, 1082−1087.
(75) Wang, L.; Huang, H.; He, T. Rayleigh Instability Induced Cylinder-to-Sphere Transition in Block Copolymer Micelles: Direct Visualization of the Kinetic Pathway. *ACS Macro Lett.* **2014**, *3*, 433−438.

https://doi.org/10.1021/jacs.1c02147
J. Am. Chem. Soc. XXXX, XXX, XXX−XXX